Chinese Chemical Letters 31 (2020) 3047–3054

Contents lists available at ScienceDirect

Chinese Chemical Letters

journal homepage: www.elsevier.com/locate/cclet

Review

Molecular engineering of C_xN_y: Topologies, electronic structures and multidisciplinary applications

Hong Yang, Zhuang Wang, Songqin Liu, Yanfei Shen, Yuanjian Zhang*

Jiangsu Engineering Laboratory of Smart Carbon-Rich Materials and Device, Jiangsu Province Hi-Tech Key Laboratory for Bio Medical Research, School of Chemistry and Chemical Engineering, Medical School, Southeast University, Nanjing 211189, China

ARTICLE INFO

Article history:
Received 6 July 2020
Received in revised form 23 July 2020
Accepted 27 July 2020
Available online 29 July 2020

Keywords:
Polymeric carbon nitrides
C_xN_y
Topology
Electronic structure
2D semiconductor

ABSTRACT

As a class of metal-free two-dimensional (2D) semiconductor materials, polymeric carbon nitrides have attracted wide attention recently due to its facile regulation of the molecular and electronic structures, availability in abundance and high stability. According to the different ratios of C and N atoms in the framework, a series of C_xN_y materials have been successfully synthesized by virtue of various precursors, which further triggers extensive investigations of broad applications ranging from sustainable photocatalytic reactions and highly sensitive optoelectronic biosensing. In view of topological structures on their electronic structures and material properties, the as-reported C_xN_y could be generally classified into two main categories with three- or six-bond-extending frameworks. Owing to the effective $n\rightarrow\pi^*$ transition in most C_xN_y materials, the relative energy level of the lone-pair electrons on N atoms is high, which thus endows the materials with the capability of visible light absorption. Meanwhile, the different repeating units, bridging groups and defect sites of these two kinds of C_xN_y allow them to effectively drive a diverse of promising applications that require specific electronic, interfacial and geometric properties. This review paper aims to summarize the recent progress in topological structure design and the relevant electronic band structures and striking properties of C_xN_y materials. In the final part, we also discuss the existing challenges of C_xN_y and outlook the prospect possibilities.

1. Introduction

From the early bronzes to modern monocrystalline silicon, novel materials with wide applications greatly promote the leap-forward development of human civilization. Among various developments, polymeric carbon nitrides composed of ubiquitous elements C and N are of enormous interest for photocatalytic water splitting [1–3] and CO_2 reduction [4,5], oxidation of small organic molecules [6–8], photoelectrochemical (PEC) [9–12] and electrochemiluminescence (ECL) [13–17] bioassay. As a metal-free polymeric semiconductor with medium-bandgap [18], the polymeric carbon nitrides materials possess a unique series of chemical and optoelectronic properties accounting for these applications. Graphitic C_3N_4 (g-C_3N_4) is the most studied polymeric carbon nitrides with exciting photocatalytic properties; however, some limitations of g-C_3N_4 still hinder their practical applications. In general, the bulk g-C_3N_4 was prepared by solid-state condensation at high-temperature, which has inherent disadvantages, including insolubility in most solvents, marginal absorption of light with wavelength more than 460 nm, the high recombination rate of charge carriers upon light irradiation, and low electrical conductivity [19]. To circumvent these limitations, the structural engineering of g-C_3N_4 by doping, controlling polymerization degree, coordinated-, covalent-, or noncovalent-functionalization, and/or tailoring nanoscale morphologies [20]. Along this line, many breakthroughs have been achieved, for instance, the quantum efficiency reached 50.7% by g-C_3N_4 in the H_2 production by photocatalytic splitting water due to the high polymerization degree [21].

In theory [22], it is also envisioned to engineer the physical/chemical properties of g-C_3N_4 by constructing unique topological structures that are closely relevant to molecular orbitals and electronic band structures. Inspired by the topologies of g-C_3N_4 and nano-carbon, a series of novel C_xN_y materials with different prosperous topologies and stoichiometries have been predicted and/or synthesized. From the perspective of molecular structures, C_xN_y materials can be divided into two catalogs, *i.e.,* three- and six-bond-extending framework, as shown in Fig. 1. For the former, triazine, tri-s-triazine, and their analogues are connected *via* three bridging N atoms, C atoms or azo linkages. The variety of repeating

* Corresponding author.
E-mail address: Yuanjian.Zhang@seu.edu.cn (Y. Zhang).

https://doi.org/10.1016/j.cclet.2020.07.048
1001-8417/

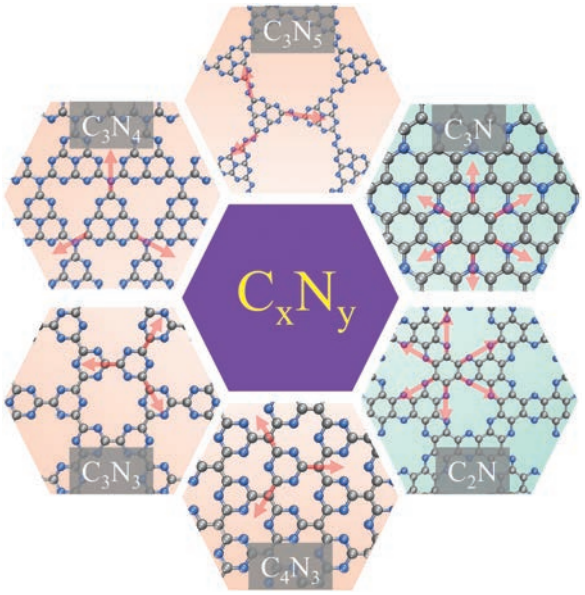

Fig. 1. Topological structures of C_xN_y. C atoms are colored in gray, while N atoms are colored in blue. The red arrows highlight the bond directions in each topological structure. The three- and six-bond-extending frameworks in different C_xN_y materials are classified by using orange and green background, respectively.

units and bridging groups determine the precise C/N ratios of each different carbon nitride, such as C_4N_3 [23], C_3N_3 [24], C_3N_4 [25] and C_3N_5 [26,27]. Nonetheless, notably, the bridging group isolates the conjugation of the π-electrons of the repeating units, thus the minimum bandgap is limited to *ca.* 1.5 eV. For the latter, the extending of benzene is achieved by the six-bonded N atoms, forming C_2N [28,29] and C_3N [30,31]. This type of framework could be regarded as that of N-doped graphene, in which, some C atoms are replaced by N atoms in a regular manner. The p_z orbitals of all C and N atoms are perpendicular to the sp^2 hybrid 2D plane, making the bandgap as low as 0.39 eV [31] and an increased conductivity surprisingly up to 1.41×10^3 S/cm after further doped by hydrochloric acid [30]. Therefore, the topological structure engineering greatly enriches the scope and the connotation of carbon nitride family both in fundamental studies and practical prospective applications.

Notably, several comprehensive and excellent feature articles have already been summarized for carbon nitride materials and their emerging applications [18–20,32–39]; nonetheless, most of them are focused specially on g-C_3N_4, and the very recent important progress on new carbon nitride family members (C_xN_y) is scarcely outlined. For this reason, this review tends to cover the recent advances of C_xN_y materials, including the relations among topological structure-electronic structure-physical/chemical properties and the prospects for wide-ranging applications advancing from energy- and environment-related topics to various new emerging fields, such as optoelectronic biosensing. In addition, this review ends with the potential aspect of the development of C_xN_y of new structures and our views on their prospective applications.

2. Strategies of topological structure engineering

In this part, we will focus on the synthesis pathway of C_xN_y materials as well as the effects of the repeating units and bridging groups on the topological structure. It should be noted that the characterization that unambiguously supports the idealized topological structure of C_xN_y materials still remains insufficient, however, typically owing to the poor solubilities and broad distribution of polymerization-degree in the same batch of products — which means some conjectures in their structures. Even so, the comprehensive analysis of topological structures plays an important role in the understanding of the C_xN_y properties.

C_3N_4 is the most reported three-bond-extending C_xN_y material. The first prediction of the topological structure of C_3N_4 was made in 1989, Liu and Cohen simulated a new hard material, β-C_3N_4 [40]. Afterward, Teter and Hemley predicted five different crystalline structures of C_3N_4 [41], which demonstrated that the g-C_3N_4 with a layered structure similar to graphite has the highest stability in the ambient condition. After that, Wolfgang Schnick and co-workers separated a stable intermediate, "melem" (2,5,8-triamino-tri-s-triazine, Fig. 2a) by thermal treatment of different less condensed C-N-H monomers (*e.g.*, cyanamide, dicyandiamide, ammonium dicyanamide or melamine) at 450 °C [25]. The nearly planar heptazine core $C_6N_7(NH_2)_3$ of the product was evidenced by X-ray powder diffractometry (XRD), and the molecular structure was revealed by solid-state nuclear magnetic resonance (NMR) spectrum, mass spectrometry (MS), Fourier transform infrared (FTIR) and Raman spectroscopy. According to the temperature-dependent XRD data, it was found that the melem was transformed into a graphite-like product at *ca.* 560 °C. Nevertheless, the accurate molecular structure of the graphite-like product has remained controversial [42–48], and two generally accepted polymerization pathways as shown in Fig. 2a, *i.e.*, tri-s-triazine-based g-C_3N_4 and triazine-based g-C_3N_4.

The 2D three-bond-extending framework consists of repeating triazine or tri-s-triazine units bridged with tertiary N atoms. Moreover, it is intriguing that the triazine-based g-C_3N_4 of high crystallinity was successfully synthesized by Bojdys and co-workers [49]. They utilized the dicyandiamide as monomers to synthesize macro-scaled crystal thin films by virtue of the ionic thermal interfacial reaction. The crystalline structure of the carbon

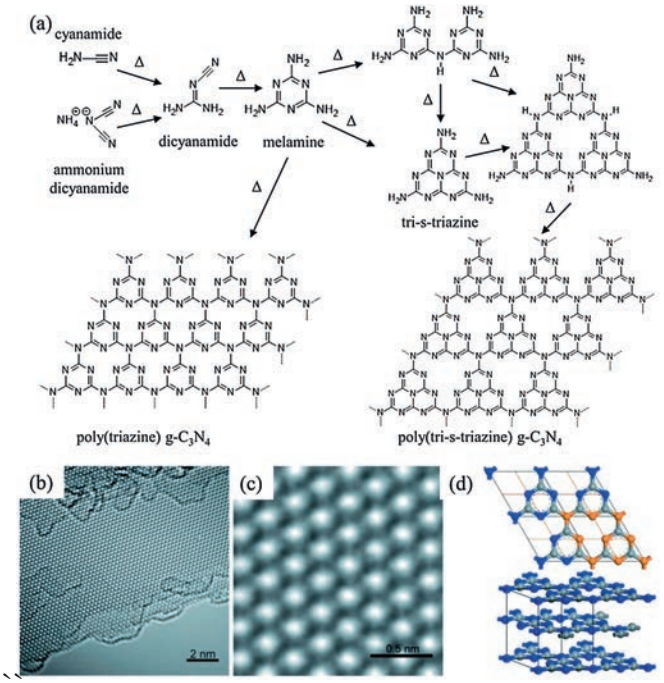

Fig. 2. Polymerization mechanism and topological structures of g-C_3N_4. (a) Proposed reaction process of triazine-based g-C_3N_4 and tri-s-triazine based g-C_3N_4. (b and c) Large crystalline thin films of triazine-based g-C_3N_4 as imaged by HR-TEM. (d) Crystallographic unit cell and AB stacking arrangement of triazine-based g-C_3N_4 layers. Orange coloring indicates a hexagonal grid of half-cell size with N atoms. Copied with permission [49]. Copyright 2014, Wiley-VCH.

nitride films was directly confirmed by high-resolution transmission electron microscope (HR-TEM, Figs. 2b and c), which was based on triazine units (Fig. 2d).

Recently, the modification in molecular structure of g-C_3N_4 has triggered enormous interests. Kumar *et al*. synthesized a novel carbon nitride framework C_3N_5 through the thermal deammoniation reaction (Fig. 3a). The monomer melem hydrazine obtained by the pre-reaction of the precursor melem and hydrazine, resulting in a new bridging azo linkage (—C=C—). It was clearly evidenced that the structure of C_3N_5 [27] is distinct from the pristine tri-s-triazine-based g-C_3N_4 by means of a variety of characterization methods, such as XRD, the electron energy loss spectroscopy (EELS), Raman spectroscopy, FTIR spectroscopy, X-ray photoelectron spectroscopy (XPS) and NMR spectrum. The overlap of tri-s-triazine heptazine cores and —C=C— linkages increased the electron density, leading to the extended conjugation and the reduction of bandgap to 1.76 eV.

Another important approach for the modification of tri-s-triazine-based g-C_3N_4 is to change the repeating units. Vinu and co-workers introduced a different topological C_3N_5 [26] with the repeating unit composed of two six-membered ring triazines and one five-membered ring triazole (Fig. 3b), which is easy to synthesize through the self-assembly of the precursor 5-amino-1*H*-tetrazole (5-ATTZ). Moreover, it was the first time that the five-membered ring structure was cooperated into C_xN_y framework. Interestingly, not only the N—N bond in the five-membered ring triazole enhanced the adsorption capacity for O_2 by adjacent active C atom sites, but also the electrons of the sp^2 hybridized N atom on the triazole moiety contributed to the π-π conjugation in the carbon nitride framework. As such, compared with bulk g-C_3N_4, the as-prepared C_3N_5 exhibited higher redox reaction activity and diffusion current density.

The repeating unit of triazine-based g-C_3N_4 also has been regarded as an intriguing model. Li and co-worker prepared C_3N_3 [24] in large scale from cyanuric chloride (Fig. 3c). One of the highlights in this work is the utilization of the Wurtz reaction, which allows simple synthesis on a copper surface under a nonvacuum condition. Different from other C_xN_y materials, both the repeating units and the bridging groups are triazine ring in C_3N_3, thereby the C—C bonds between triazine rings constructs the framework. It is similar to C_3N_5, when the bridging group is changed from N atom to C atom leading to C_4N_3 (Fig. 3d) [23], synthesized by Zhou *et al*. It is worthwhile pointing out that some unoccupied electrons may exist in the bridging C atoms, resulting in more dangling bonds and subsequent much improved optical absorption.

It has gained significant interest to assemble 2D single crystals synthesized from other elements besides C atoms, which was initially reported by Baek and co-workers. They selected hexaaniline as the precursor, and obtained two kinds of six-bond-extending 2D ordered crystals with the empirical formulas of C_2N [28] and C_3N [30]. Meanwhile, they predicted that these materials with unique geometric and electronic band structures would open up new opportunities for materials science, thereby broadening the application range from electronics, sensors, catalysis to wider research fields [50,51].

The monomers including hexaaminobenzene (HAB) trihydrochloride and hexaketocyclohexane (HKH) octahydrate were selected for spontaneous polycondensation to form a single crystalline material called C_2N-*h*2D (C_2N holey 2D crystal, Fig. 4a). In the layered structure with high crystallinity of C_2N, sub-nanometer holes were constructed from phenyl rings and directional N atoms. More specifically, each phenyl ring bridged six common secondary N atoms and shared them with another phenyl ring, thereby the framework extending was achieved by two adjacent N atoms. The holey structure in hexagonal arrays was evidenced by various characterization methods, *e.g*., XRD, XPS and EELS spectroscopy and scanning tunneling microscope (STM, Fig. 4b) based on a single-layer crystal sample loading on the Cu (111) substrate.

The single crystal of C_3N was synthesized by a direct pyrolysis of the HAB trihydrochloride (Fig. 4c). The 2D sheet-like appearance without any hole in C_3N was formed by three sp^2 hybrid C atoms (from different phenyl rings) and a shared tertiary N atom. This interesting structure was verified by using solid-state ^{13}C NMR spectrum and STM. Only two peaks were observed in the ^{13}C NMR spectrum, which assigned to the C atoms covalently bonded with tertiary N atoms in the basal plane and the C atoms attached to

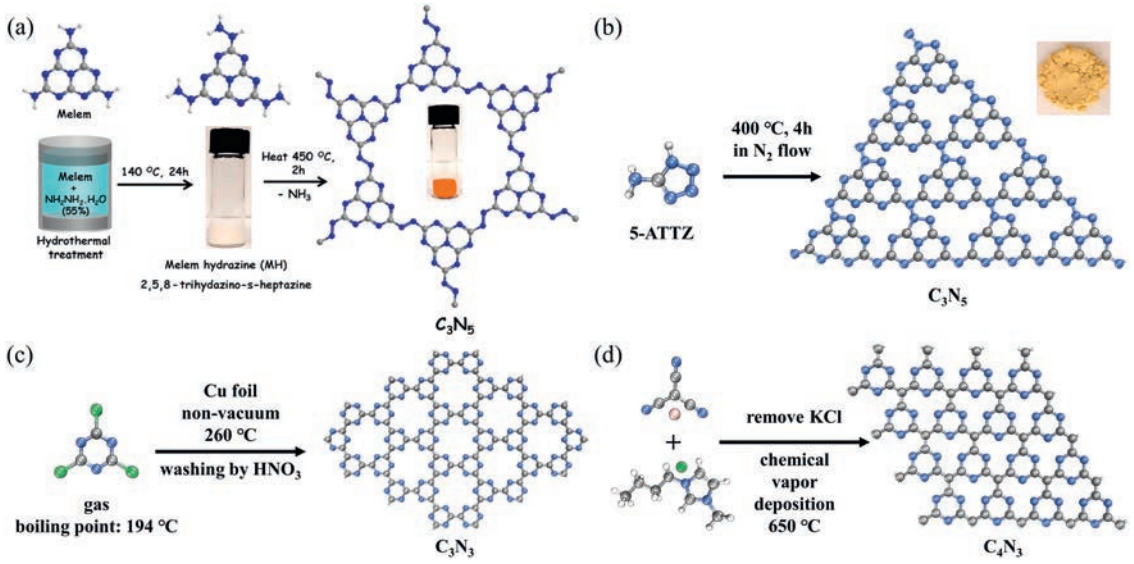

Fig. 3. Synthesis pathway and topological structures of three-bond-extending C_xN_y materials. (a) Synthesis pathway of C_3N_5 from melem and hydrazine *via* the melem hydrazine obtained by pre-reaction. Different to that of tri-s-triazine based g-C_3N_4, the bridging unit of C_3N_5 is changed into azo linkage. The distinct colors of the precursor and product as shown in the vials. Copied with permission [27]. Copyright 2019, American Chemical Society. (b) The polymerization of C_3N_5 (changed repeating unit compared with tri-s-triazine-based g-C_3N_4) from precursor 5-ATTZ. The powder products as shown in the top-right inset. Copied with permission [26]. Copyright 2018, Wiley-VCH. The synthesis pathways of (c) C_3N_3 and (d) C_4N_3 from the vapor of precursors. Cl atoms are colored in green, while K atoms are colored in pink.

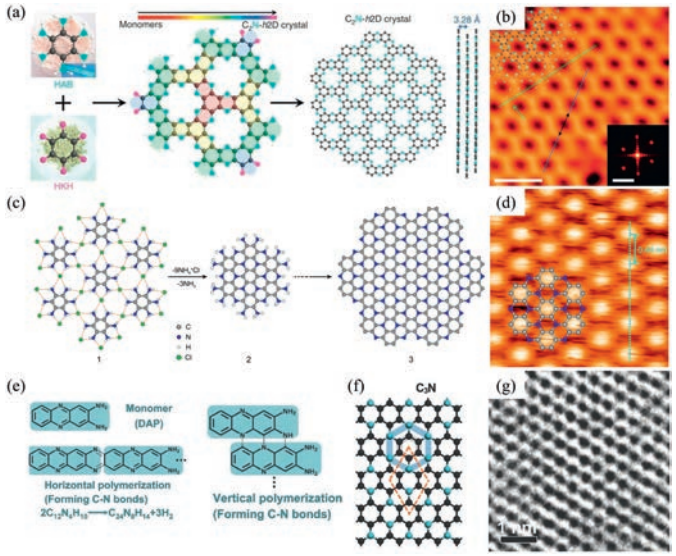

Fig. 4. Synthesis pathway and topological structures of the crystals, C_2N and C_3N. (a) The synthesis pathway of the crystal C_2N from HAB and HKH. (b) An atomic-resolution STM topography image of the crystal C_2N. The top-left inset structure represents its repeating unit. The bottom-right inset is 2D fast Fourier transform. The scale bars in the picture and inset are 2.0 nm and 2.0 nm^{-1}, respectively. Copied with permission [28]. Copyright 2015, Nature publishing group. (c) The synthesis pathway of the crystal C_3N from HAB. (d) STM image of a crystal C_3N framework. Inset: The structure of the crystal C_3N superimposed on the image. Copied with permission [30]. Copyright 2016, National Academy of Sciences. (e) Polymerization scheme of DAP with the formation of C—N bonds through the horizontal direction (abstraction of H from C—H and N—H bonds) and vertical direction. (f) The topology structure and supercell (red dotted diamond) of the crystal C_3N framework. (g) Spherical aberration-corrected HR-TEM image shows the honeycomb structure of C_3N nanosheets. Copied with permission [31]. Copyright 2015, Wiley-VCH.

primary or secondary amine groups at the edges, respectively. Moreover, the well-ordered structure of C_3N was revealed on STM (Fig. 4d), which was regarded as a perfect graphene analogue with some C atoms regularly replaced by N atoms. Nevertheless, the application of the produced C_2N and C_3N was limited because of the high cost of the precursor of HAB.

Another 2D crystalline C_3N [31] with the same molecular structure was fabricated through the hydrothermal treatment of the monomer, 2,3-diaminophenazine (DAP, Fig. 4e) by Kang and co-workers. Both single-crystalline sheets with hundreds of micrometers size and hexagonal quantum dots (QDs) with nanometer size of C_3N were successfully prepared by solvothermal reactions (250–400 °C) under a home-made high-pressure container. The well-defined 2D single crystalline structure is illustrated in Fig. 4f, where N atoms and C atoms are evenly distributed in a 2D plane with D_{6h} symmetry. The specific structure of C_3N sheets was disclosed by TEM, STM, XRD, Raman and NMR spectrum. The spherical aberration-corrected HR-TEM image (Fig. 4g) of a single-layer sheet evidently showed the well-crystallized six-bond-extending honeycomb structure.

Nonetheless, a major limitation for large-scale application of single crystal C_xN_y materials exists, owing to the high-cost precursors and dangerous reaction conditions. An important advance by simple, economical and practical reaction methods for C_xN_y was pioneered by Antonietti and co-workers [29]. For instance, the mixtures of phenols/ketones and urea exhibited eutectic behavior upon mild heating. These mixtures possess liquid-crystalline-like phases (Fig. 5a) that can be processed. As a specific example, condensation of HKH and urea at elevated temperatures resulted in remarkably high N content of product with the approximate composition of C_2N (Fig. 5b). Carbonaceous intermediates with metallic-gloss were obtained starting from reaction temperatures as low as 500 °C. The product condensed at 700–800 °C was described as a disordered C_2N with the N content of 28 wt%. In this reaction, the architecture of HKH served as a structure-donating motif, while urea acted simultaneously as a melting-point reduction agent and N source. It was revealed that the condensation of precursors occurred in a structurally organized fashion, in which N atoms were predominately placed in pyrazinic positions, with pyrrolic N presented for surface termination and as defect sites.

From the perspective of topological structures, different precursors endow different repeating units and different numbers of bridging groups, which further determine the extending manner. Notably, the repeating units of three-bond-extending C_xN_y materials have a more diverse selection, such as symmetric triazine, tri-s-triazine and asymmetric unit composed of two triazines and one triazole. The bridging groups can also be N atom or azo linkage. On this basis, 2D materials containing nanoscale holes in the repeating cells were constructed. In contrast, six-bond-extending C_xN_y materials can only be constructed by the repeating unit of the phenyl rings and bridging groups of N atoms. It is because the phenyl ring has the ability to extend six directions through valence bonds, and the larger bridging groups (more steric hindrance) are difficult to assemble into the C_xN_y framework.

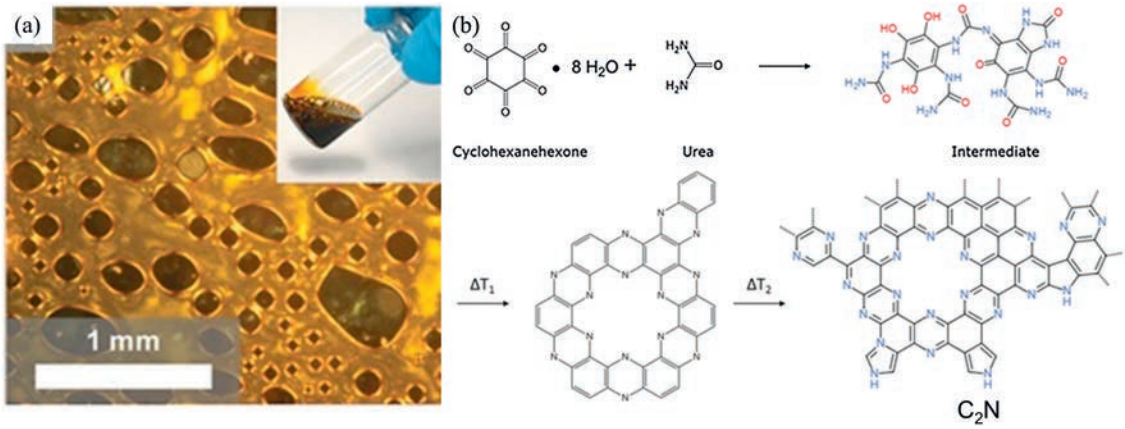

Fig. 5. Synthesis pathway and molecular structures of disordered C_2N. (a) The liquid-crystalline eutectic intermediate observed by optical microscopy in the supercooled liquids, partial polarization mode (inset: macroscopic photograph). (b) Synthesis pathway of disordered C_2N (bottom) from HKH and urea *via* a liquid-crystalline eutectic intermediate (top) obtained by pre-reaction. Copied with permission [29]. Copyright 2015, Wiley-VCH.

Therefore, the molecular structure with the π-electron cloud across the 2D framework of the latter materials is more similar to that of graphene.

3. Electronic band structures of C_xN_y

In this section, we will discuss the connections between the topology, frontier orbitals and electronic band structures of different C_xN_y materials based on different calculation theories. It should be noted that the richer kinds of topology of the C_xN_y family were, the more diverse the corresponding electronic band structures were, resulting in prosperous applications.

Wang *et al.* calculated the highest occupied molecular orbital/lowest unoccupied molecular orbital (HOMO–LUMO gap) of the precursor and linear tri-s-triazine-based g-C_3N_4 [1], which decreased from 3.5 eV (melem molecule) *via* 2.6 eV (polymeric melon) to 2.1 eV (infinite 2D sheet). Although the value of the bandgap was underestimated, it was consistent with the characteristics of the DFT method and the selected HOMO-LUMO gap model, supporting the trend in the UV–vis experiments. The polymeric melon with a non-isotropic band structure (direct bandgap at the Γ point, Fig. 6a) dispersed along the Γ-X direction parallel to the chain. The isosurfaces of the valence band maximum (VBM, Fig. 6b) and the conduction band minimum (CBM, Fig. 6c) were mainly consists of nitrogen p_z orbitals and carbon p_z orbitals, respectively. Given the positions of both VBM and CBM, it was predicted that the N atoms provided the oxidation site for H_2O to generate O_2, while the C atoms offered a reduction site for H^+ to generate H_2 under the photoexcitation.

In another interesting work, Vinu and co-workers prepared triazole-based C_3N_5 [26] monolayer (triclinic lattice, Fig. 6d), a three-bond-extending carbon nitride, and the calculated interatomic distances and lattice parameters were matched well with the experimental data. The charge distribution of C_3N_5 (Figs. 6e and f) demonstrated that the most positive potential in this structure appeared on the C1 and C4 atoms with an electron-deficient state, thus explaining the enhancement of the redox reaction by virtue of the intrinsic electron density (partially negative) in the N atom site. Moreover, this was the first report which implied the effect of the five-membered ring molecule implanted to the repeating unit in C_xN_y materials.

In view of electronic structures, the topology of the six-bond-extending C_xN_y materials not only inherits some unique features of graphene, but also endows the uniform distribution of N atoms intriguingly accounting for emerging multi-functional properties. Baek and co-workers adopted the gradient-corrected DFT calculation for the six-bond-extending crystal materials, C_2N-*h*2D [28] and C_3N [30] to determine the electronic band structures. The results showed that the bandgap of C_2N 2D triangular lattice was *ca.* 1.70 eV (Figs. 7a and b), which was matched with the optical data (1.96 eV) very well. The CBM (Fig. 7c) and VBM (Fig. 7d) were predominantly derived from N atoms. As for the former one, the flat band consisted of the local p-orbital and a non-localized dispersion band across the entire plane. While the double-degenerate flat band consisted of the non-bonded σ-orbital in the latter one. The simulated STM image of C_3N was also revealed by DFT calculation (Fig. 7e), and the theoretical lattice constant was 475 pm, slightly higher (by approximately 35 pm) than the experimental value. The calculated Brillouin zone (Fig. 7f) showed that C_3N had a nonzero finite density of states close to the Fermi level, which was in agreement with the result of scanning tunneling spectroscopy. The VBM originated from the p_z orbitals of the C atoms, while the CBM derived from the p_z orbitals of the C atoms (Fig. 7g).

Another C_3N [31] material synthesized by Kang and co-workers was determined to be an indirect energy bandgap semiconductor with a bandgap of 0.39 eV by DFT calculation (Fig. 7h), which was unusually reported in conventional 2D carbon-based materials. The VBM and CBM were located at the M point and the Γ point, respectively. Moreover, the calculated and measured data of size-dependence bandgap increased with the reduction of the QDs diameter. When the size of QDs was smaller than 1.8 nm, the bandgap outstripped 2.74 eV (Fig. 7i).

By comparison, it is obvious to find the similarities and differences between three-and six-bond-extending C_xN_y through topology and electronic band structures. In general, the same aspect is that the VBM and CBM of the two types of materials

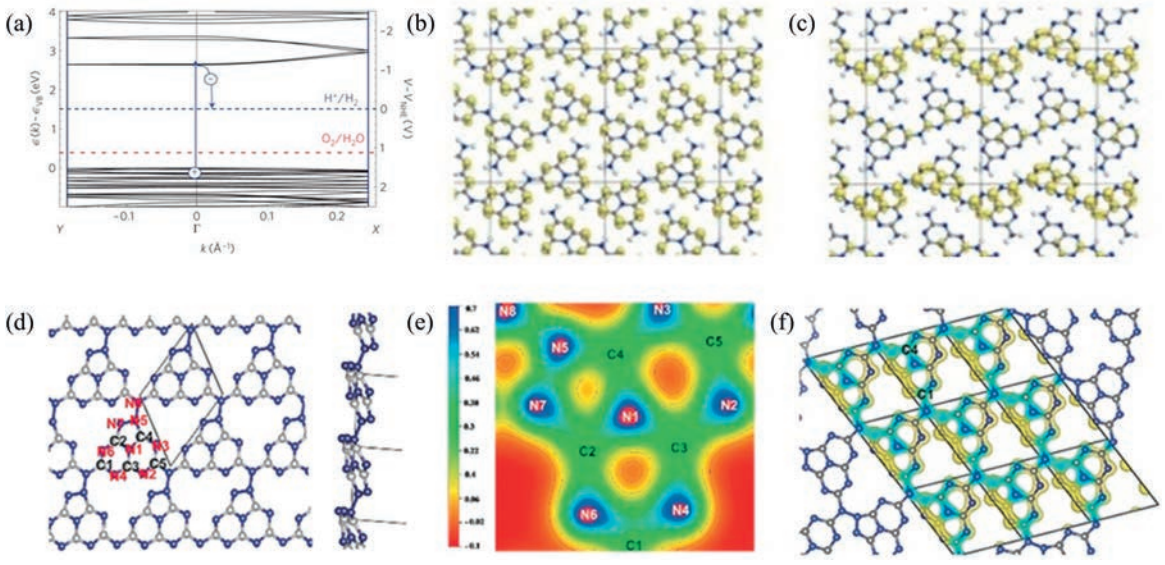

Fig. 6. Electronic band structures of the linear tri-s-triazine-based g-C_3N_4 and C_3N_5. (a) DFT band structure for linear tri-s-triazine-based g-C_3N_4. The position of the reduction potential of H^+ to H_2 and the oxidation potential of H_2O to O_2 are indicated by the blue and red dashed lines, respectively. Isosurfaces of the (b) valence band and (c) conduction band of linear tri-s-triazine-based g-C_3N_4 with charge density of 0.01 q_e /Å^3. Copied with permission [1]. Copyright 2008, Nature publishing group. DFT calculation results of C_3N_5. (d) Optimized chemical structure, (e) 2D contour representation charge density distribution in [001] plane and (f) 3D isosurface with charge density of 0.02 q_e /Å^3. Yellow coloring indicates electron-rich areas and cyan indicates the electron-deficient areas. Copied with permission [26]. Copyright 2018, Wiley-VCH.

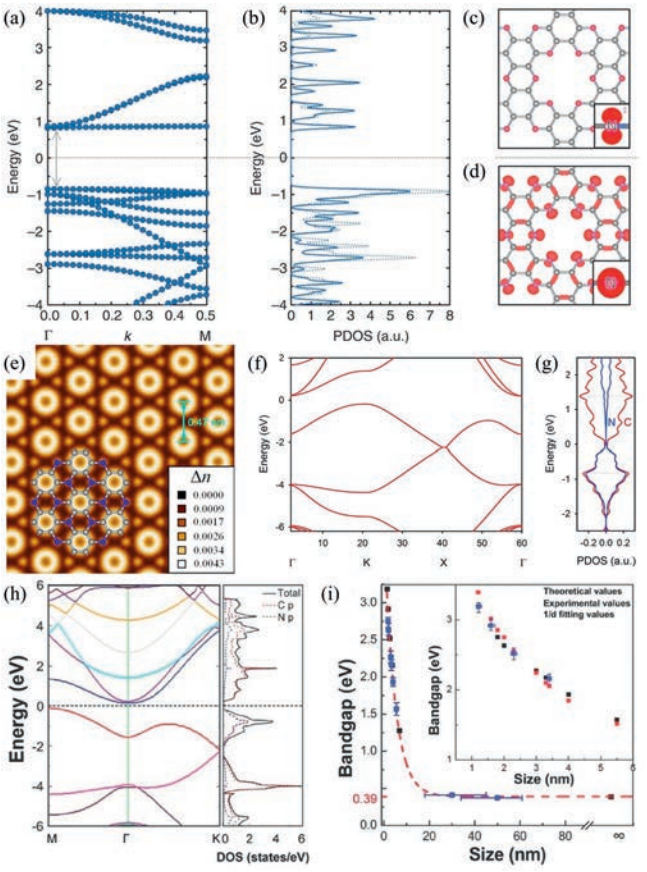

Fig. 7. Electronic band structures of C_3N and C_2N crystal. (a) The band structure, (b) the density of electronic states, and isosurfaces according to (c) the conduction-band minimum state and (d) valence-band maximum state of C_2N 2D triangular lattice. Copied with permission from [28]. Copyright 2015, Nature publishing group. (e) The simulated STM image, (f) electronic band structure and (g) projected density of electronic states of C_3N repeating unit with the superimposed structure. Copied with permission from [30]. Copyright 2016, National Academy of Sciences. (h) The electronic band structure of C_3N with a single-layer. (i) The energy bandgap (black: calculated data and blue: experimental data) of size-dependence C_3N QDs. The inset shows the changes of bandgap values following the size of QDs diameters (1/d). Copied with permission [31]. Copyright 2015, Wiley-VCH.

compose of p_z orbitals of N atoms and C atoms, respectively, leading to a medium-sized bandgap. This feature is predominantly caused by the high energy level of the non-bonded orbital occupied by the lone pair of electrons on the N atom in the six-membered ring repeating units. That is, the dominant form of electronic transition in most C_xN_y materials is the $n\rightarrow\pi^*$ transition. Meanwhile, one of the different aspects is reflected in that the three-bond-extending materials are difficult to form a large 2D conjugate plane due to the blocking bridging units, resulting in a rare production of macroscopic sized crystals. On the other hand, these bridging units and defect sites (*e.g.*, $-NH_2$ terminal group) would in turn be the active sites in photo-/electronic-catalysis. Therefore, the two types of materials with different properties are blossoming in multidisciplinary applications.

4. Applications of C_xN_y

Owing to the diverse molecular and electronic structures, C_xN_y has gained a very broad scope of applications. Many comprehensive review articles [18–20,32–39] have already given excellent summaries, hence, only a minor portion of presentative works are discussed here. The g-C_3N_4 material was first used as heterogeneous catalysis [52] in 2006, ten years after the theoretical prediction of its structure. It was regarded as a milestone that Thomas, Antonietti and co-workers constructed a metal-free catalyst for the Friedel-Crafts acylation reaction by using mesoporous g-C_3N_4 (Fig. 8a). The reaction is speculated as to the electron transition from the HOMO of g-C_3N_4 to the LUMO of benzene, resulting in the activation of the phenyl ring. Subsequently, Wang *et al.* applied g-C_3N_4 in producing H_2 (Fig. 8b) from photocatalytic water splitting as a metal-free semiconductor photocatalyst [1] for the first time in 2009. Accompanied by the sacrificial agent triethanolamine and the co-catalyst Pt, the quantum efficiency of g-C_3N_4 increased to 0.1% under the visible-light irradiation. In the same year, the photocurrent generation of g-C_3N_4 was reported by our group and later with improved efficiencies by photoelectrode optimization (Fig. 8c) [53]. Notably, Shalom proposed a pre-organization of monomers and thermal evaporation method to strengthen the deposition interface of g-C_3N_4 on fluorine-doped tin oxide (FTO) glass, resulting in substantially improved PEC efficiencies [54].

In addition, owing to unique electronic band structures in electrical-optical interconversion and electrocatalysis, g-C_3N_4 has been widely used as an electrode material for bioassay in the form of PEC sensing and ECL. For example, our group has reported that the CN_{MW} (carbon nitride prepared by microwave-assisted condensation) photoelectrode displayed a record-level cathodic efficiency of ECL up to 7 times that of standard $Ru(bpy)_3Cl_2$ (Fig. 8d) [17] in aqueous solution. As an important advance by CN photoelectrode, we developed a biomimetic ECL biosensor for 8-hydroxy-2′-deoxyguanosine (8−OHdG, an important biomarker for DNA oxidative damage) based on two competitive mechanisms involving steric hindrance and catalysis by assembling hemin/G-quadruplex on carbon nitride nanosheets (Fig. 8e) [55]. The detection limit was as low as 38.8 amol/L, which is much lower than those for the best previously reported biosensors. For other three-bond-extending C_xN_y, the mesoporous C_3N_5 exhibited the CO_2 capturing capacity of 5.63 mmol/g [56], and higher activity in oxygen reduction reaction (Fig. 8f) [26].

The six-bond-extending C_xN_y also holds huge promise in other emerging fields of renewable resources not merely as a semiconductor. Compared with the undoped C_3N, it was found by Baek and co-workers that the conductivity was set as high as 1.41×10^3 S/cm after doping it with hydrochloric acid [30], which is the highest value among organic materials to date. Thus, C_3N and C_2N with a layered 2D framework were reported to own excellent electrochemical activities as anode materials in lithium-ion batteries [50], including high reversible capacities, low voltage hysteresis, efficient operating voltage window, and excellent cycling stability. The unique electronic structure based on C_3N was supposed to account for the structural stability, enhanced net positive charge densities, and high electronic/ionic conductivity (Fig. 8g). Moreover, due to the flexible bandgaps, Kang and co-workers developed C_3N QDs of different sizes with photoluminescent emission covered the entire visible range (450−790 nm) and successfully applied them in bioimaging (Fig. 8h) [31].

5. Summary and perspectives

The C_xN_y materials are easy to synthesize from various precursors, and their final structures depend on the choice of monomers. Specifically, the changes of bridging groups and repeating units in the three-bond-extending structures greatly enrich the varieties of topology. Moreover, the phenyl rings in six-bond-extending structures that is bridged by N atoms leads to a 2D conjugate plane, in which, the quantity and the linkage modes of N atoms determine the extension manner of the phenyl ring. The prosperous topological structures determine the electronic band structures, realizing the wide coverage of C_xN_y materials in the

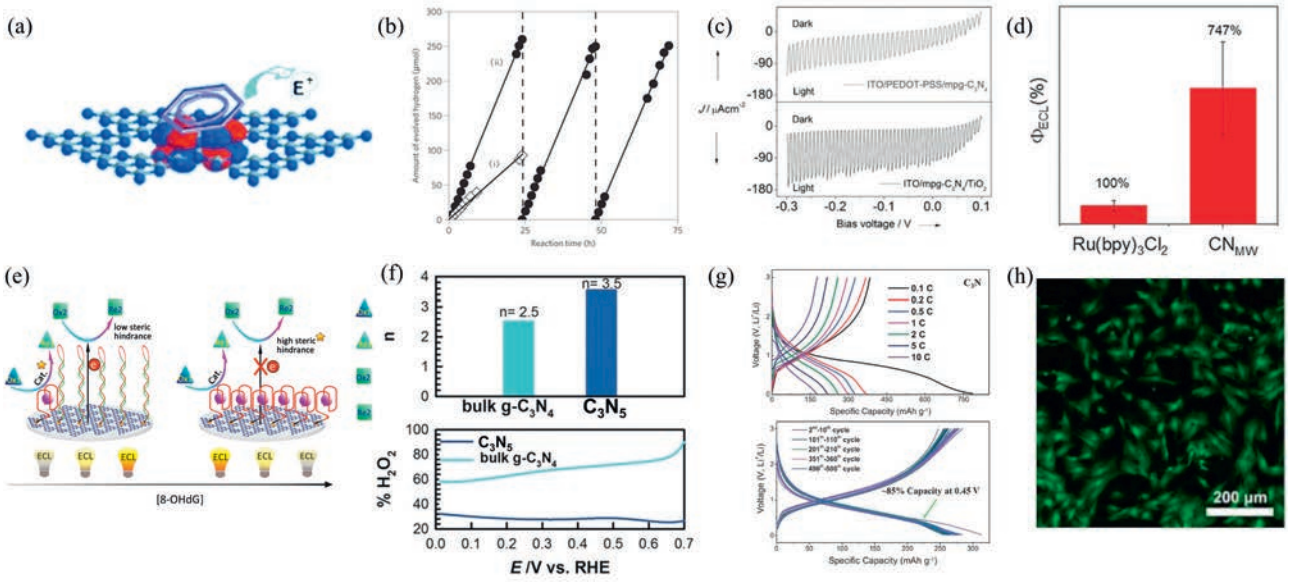

Fig. 8. Diverse applications of C_xN_y. (a) The proposed catalytic mechanism arises from a shift of electron density from the HOMO of g-C_3N_4 to the LUMO of benzene. Copied with permission from [52]. Copyright 2006, Wiley-VCH. (b) A typical time course of H_2 production from water containing triethanolamine as sacrificial agent under visible light (λ > 420 nm) by (i) unmodified g-C_3N_4 and (ii) g-C_3N_4 modified by co-catalyst Pt. Copied with permission [1]. Copyright 2008, Nature publishing group. (c) Linear sweep voltammetry curves under visible light (λ > 420 nm) by ITO/PEDOT-PSS/mpg-C_3N_4 and ITO/mpg-C_3N_4/TiO_2. Copied with permission [53]. Copyright 2010, Wiley-VCH. (d) ECL efficiency of CN_{MW} and benchmark $Ru(bpy)_3Cl_2$. Copied with permission [17]. Copyright 2019, Wiley-VCH. (e) Proposed reactions occurring at the dual-mechanism-driven biosensor at (left) low and (right) high concentrations of 8−OHdG. Copied with permission [55]. Copyright 2018, American Chemical Society. (f) Electron transfer number (top) and HO_2^- yield (bottom) of bulk g-C_3N_4 and C_3N_5. Copied with permission [26]. Copyright 2018, Wiley-VCH. (g) Charge/discharge profiles and of C_3N at various C-rates (top) and 1 C (bottom). Copied with permission [50]. Copyright 2017, Wiley-VCH. (h) Bright fluorescence image (using C_3N QDs) of tissue-derived stromal cells. The bright spots are cell nuclei. They are surrounded by less intense areas which are the cells. Copied with permission [31]. Copyright 2015, Wiley-VCH.

bandgap range of *ca.* 0.4−3 eV. As such, the C_xN_y materials own extremely wide application scenarios ranging from photocatalysis, electrocatalysis to battery electrodes and from biosensing to other new fields.

It is worth noting that the more these kinds of materials were researched, the more unexpected surprises and performance records could be found. Nonetheless, there are still some challenges to be solved:

(i) C_xN_y materials except for g-C_3N_4 have been synthesized in the past five years. Thereby, they drew much less attention than g-C_3N_4 that has almost been the alias for the carbon nitrides family. On the one hand, these materials are rarely reported by other groups apart from the groups who have originally synthesized those. On the other hand, both the difficulties and the high cost of synthesis of C_xN_y (except for g-C_3N_4), which confined their applications. Besides, narrowed band-gaps are preferred for solar fuel or optoelectronic applications, but fewer practical successful examples have been demonstrated for C_xN_y (*e.g.*, C_3N, C_3N_5, C_3N_2). Therefore, a more fundamental understanding and the optimal application of each material are still under exploration in experiments and theories.

(ii) So far, six-membered rings are still the main repeating units of the C_xN_y family, and the carbon nitride materials based on five-membered rings as the repeating units are still in their infancy. Tsetseris has proposed the possibility of the polymerization of tetracyanoethylene into a stable five-membered ring-based phthalocyanine-like polymeric carbon nitrides framework by virtue of the DFT calculation [57]. Although the precursor as well as the ratio of C and N atoms of the product in this model are similar to that in an earlier experimental report [58], the calculated properties are not fully matched to the experiment. Very recently, our groups synthesized a five-membered ring-based C_3N_2 material by using the zeolite imidazole framework [59]. The asymmetric five-membered rings and the rich dangling bonds in the condensed framework endow much lower first excitation energy of 0.8 eV, enabling the first successful PEC biosensing for the untransparent biological samples using near IR lights. All these unique features suggest the great potential of studying the five-membered ring C_xN_y material with attractive future applications.

(iii) The first exciting application of polymeric carbon nitride was its great potential in photocatalytic water splitting. Although the efficiency was not among the state-of-the-art, it has led a new field in catalyzing water splitting reactions by using visible light and a metal-free semiconductor, which is extremely important for both fundamental research and developing next generation of strategies to address the challenge of sustainable energy. An exceptional example was reported very recently for polymeric carbon nitride in the interconversion between different types of energy. The carbon nitride photoelectrode by an ultrafast thermal condensation already demonstrated a record-level cathodic efficiency (Fig. 8d) in aqueous solution, which is highly envisioned to be further explored as a killer application.

In the past two decades, enormous advances have been achieved for C_xN_y family both in theoretical studies and practical applications. We speculate that more exciting properties of carbon nitride would be discovered, which appeal for the participation of more researchers from multidisciplinary fields. It is envisioned that this review can provide a useful perspective for this field and promote the exploration of C_xN_y with more abundant topological structures, electronic band structure, novel properties, and multiple application prospects.

Declaration of competing interest

The authors declare that they have no known competing financial interests or personal relationships that could have appeared to influence the work reported in this paper.

Acknowledgments

This work was supported by the National Natural Science Foundation of China (Nos. 21775018, 21675022), the Natural Science Foundation of Jiangsu Province (No. BK20170084), the Open Funds of the State Key Laboratory of Electroanalytical Chemistry (No. SKLEAC201909), and the Fundamental Research Funds for the Central Universities.

References

[1] X. Wang, K. Maeda, A. Thomas, et al., Nat. Mater. 8 (2009) 76–80.
[2] J. Liu, Y. Liu, N. Liu, et al., Science 347 (2015) 970–974.
[3] R. Godin, Y. Wang, M.A. Zwijnenburg, J. Tang, J.R. Durrant, J. Am. Chem. Soc. 139 (2017) 5216–5224.
[4] G. Gao, Y. Jiao, E.R. Waclawik, A. Du, J. Am. Chem. Soc. 138 (2016) 6292–6297.
[5] R. Kuriki, H. Matsunaga, T. Nakashima, et al., J. Am. Chem. Soc. 138 (2016) 5159–5170.
[6] Y. Wang, X. Wang, M. Antonietti, Angew.Chem. Int. Ed. 51 (2012) 68–89.
[7] S. Cao, J. Low, J. Yu, M. Jaroniec, Adv. Mater. 27 (2015) 2150–2176.
[8] Y. Zhao, M. Antonietti, Angew.Chem. Int. Ed. 56 (2017) 9336–9340.
[9] A.J. Bard, Science 207 (1980) 139–144.
[10] M. Grätzel, Nature 414 (2001) 338–344.
[11] Y. Zhang, M. Antonietti, Chem. Asian J. 8 (2010) 1307–1311.
[12] Y. Fang, Y. Xu, X. Li, Y. Ma, X. Wang, Angew.Chem. Int. Ed. 57 (2018) 9749–9753.
[13] P. Wu, X. Hou, J.J. Xu, H.Y. Chen, Chem. Rev. 114 (2014) 11027–11059.
[14] J. Ji, J. Wen, Y. Shen, et al., J. Am. Chem. Soc. 139 (2017) 11698–11701.
[15] L. Li, Y. Chen, J.J. Zhu, Anal. Chem. 89 (2017) 358–371.
[16] Y. Lv, S. Chen, Y. Shen, et al., J. Am. Chem. Soc. 140 (2018) 2801–2804.
[17] T. Zhao, Q. Zhou, Y. Lv, et al., Angew.Chem. Int. Ed. 59 (2020) 1139–1143.
[18] J. Liu, H. Wang, M. Antonietti, Chem. Soc. Rev. 45 (2016) 2308–2326.
[19] W.J. Ong, L.L. Tan, Y.H. Ng, S.T. Yong, S.P. Chai, Chem. Rev. 116 (2016) 7159–7329.
[20] Z. Zhou, Y. Zhang, Y. Shen, S. Liu, Y. Zhang, Chem. Soc. Rev. 47 (2018) 2298–2321.
[21] L. Lin, H. Ou, Y. Zhang, X. Wang, ACS Catal. 6 (2016) 3921–3931.
[22] K. Fukui, T. Yonezawa, H. Shingu, J. Phys. Chem. C 20 (1952) 722–725.
[23] G. Zhou, Y. Shan, Y. Hu, et al., Nat. Commun. 9 (2018) 3366.
[24] J. Feng, M. Li, Adv. Funct. Mater. 30 (2020) 2001502.
[25] B. Jürgens, E. Irran, J. Senker, et al., J. Am. Chem. Soc. 125 (2003) 10288–10300.
[26] I.Y. Kim, S. Kim, X. Jin, et al., Angew. Chem. Int. Ed. 57 (2018) 17135–17140.
[27] P. Kumar, E. Vahidzadeh, U.K. Thakur, et al., J. Am. Chem. Soc. 141 (2019) 5415–5436.
[28] J. Mahmood, E.K. Lee, M. Jung, et al., Nat. Commun. 6 (2015) 6486.
[29] N. Fechler, N.P. Zussblatt, R. Rothe, et al., Adv. Mater. 28 (2016) 1287–1294.
[30] J. Mahmood, E.K. Lee, M. Jung, et al., Proc. Natl. Acad. Sci. U. S. A. 113 (2016) 7414–7419.
[31] S. Yang, W. Li, C. Ye, et al., Adv. Mater. 29 (2017) 1605625.
[32] Y. Zheng, J. Liu, J. Liang, M. Jaroniec, S.Z. Qiao, Energy Environ. Sci. 5 (2012) 6717–6731.
[33] X.-H. Li, M. Antonietti, Chem. Soc. Rev. 42 (2013) 6593–6604.
[34] J. Zhang, Y. Chen, X. Wang, Energy Environ. Sci. 8 (2015) 3092–3108.
[35] Z. Zhao, Y. Sun, F. Dong, Nanoscale 7 (2015) 15–37.
[36] F.K. Kessler, Y. Zheng, D. Schwarz, et al., Nat. Rev. Mater. 2 (2017) 17030.
[37] K.S. Lakhi, D.-H. Park, K. Al-Bahily, et al., Chem. Soc. Rev. 46 (2017) 72–101.
[38] T.S. Miller, A.B. Jorge, T.M. Suter, et al., Phys. Chem. Chem. Phys. 19 (2017) 15613–15638.
[39] G. Zhang, Z.-A. Lan, X. Wang, Chem. Sci. 8 (2017) 5261–5274.
[40] A.Y. Liu, M.L. Cohen, Science 245 (1989) 841–842.
[41] D.M. Teter, R.J. Hemley, Science 271 (1996) 53–55.
[42] E.G. Gillan, Chem. Mater. 12 (2000) 3906–3912.
[43] Z. Zhang, K. Leinenweber, M. Bauer, et al., J. Am. Chem. Soc. 123 (2001) 7788–7796.
[44] D.R. Miller, J. Wang, E.G. Gillan, J. Mater. Chem. 12 (2002) 2463–2469.
[45] E. Kroke, M. Schwarz, Coord. Chem. Rev. 248 (2004) 493–532.
[46] D.R. Miller, D.C. Swenson, E.G. Gillan, J. Am. Chem. Soc. 126 (2004) 5372–5373.
[47] B.V. Lotsch, M. Döblinger, J. Sehnert, et al., Chem. Eur. J. 13 (2007) 4969–4980.
[48] A. Thomas, A. Fischer, F. Goettmann, et al., J. Mater. Chem. 18 (2008) 4893–4908.
[49] G. Algara-Siller, N. Severin, S.Y. Chong, et al., Angew. Chem. Int. Ed. 53 (2014) 7450–7455.
[50] J. Xu, J. Mahmood, Y. Dou, et al., Adv. Mater. 29 (2017) 1702007.
[51] J. Mahmood, F. Li, S.-M. Jung, et al., Nat. Nanotechnol. 12 (2017) 441–446.
[52] F. Goettmann, A. Fischer, M. Antonietti, A. Thomas, Angew. Chem. Int. Ed. 45 (2006) 4467–4471.
[53] Y. Zhang, A. Thomas, M. Antonietti, X. Wang, J. Am. Chem. Soc. 131 (2009) 50–51.
[54] G. Peng, J. Albero, H. Garcia, M. Shalom, Angew. Chem. Int. Ed. 57 (2018) 15807–15811.
[55] Y. Lv, S. Chen, Y. Shen, et al., J. Am. Chem. Soc. 140 (2018) 2801–2804.
[56] D.H. Park, K.S. Lakhi, K. Ramadass, et al., Chem. Eur. J. 23 (2017) 10753–10757.
[57] L. Tsetseris, 2d Mater. 3 (2016) 021006.
[58] H. Yanagi, H. Itoh, Y. Ueda, M. Ashida, Appl. Phys. Lett. 65 (1994) 1909–1911.
[59] H. Yang, Q. Zhou, Z. Fang, et al., ChemRxiv (2020), doi:http://dx.doi.org/10.26434/chemrxiv.12195429.